Seasonal Variations of Stratospheric Age Spectra in GEOSCCM

Li, Feng[1,2], Darryn Waugh[3], Anne R. Douglass[2], Paul A. Newman[2], Steven Pawson[2], Richard S. Stolarski[2,3], Susan E. Strahan[1,2], J. Eric Nielsen[2,4]

[1]NASA Goddard Earth Sciences Technology and Research, Greenbelt, MD, USA
[2]NASA Goddard Space Flight Center, Greenbelt, MD, USA
[3]Johns Hopkins University, Baltimore, MD, USA
[4]Science Systems and Application Inc., Lanham, MD USA

Popular Summary

There are many pathways for an air parcel to travel from the troposphere to the stratosphere, each of which takes different time. The distribution of all the possible transient times, i.e. the stratospheric age spectrum, contains important information on transport characteristics. However, it is computationally very expensive to compute seasonally varying age spectra, and previous studies have focused mainly on the annual mean properties of the age spectra. To date our knowledge of the seasonality of the stratospheric age spectra is very limited.

In this study we investigate the seasonal variations of the stratospheric age spectra in the Goddard Earth Observing System Chemistry Climate Model (GEOSCCM). We introduce a method to significantly reduce the computational cost for calculating seasonally dependent age spectra. Our simulations show that stratospheric age spectra in GEOSCCM have strong seasonal cycles and the seasonal cycles change with latitude and height. In the lower stratosphere extratropics, the average transit times and the most probable transit times in the winter/early spring spectra are more than twice as old as those in the summer/early fall spectra. But the seasonal cycle in the subtropical lower stratosphere is nearly out of phase with that in the extratropics. In the middle and upper stratosphere, significant seasonal variations occur in the subtropics. The spectral shapes also show dramatic seasonal change, especially at high latitudes. These seasonal variations reflect the seasonal evolution of the slow Brewer-Dobson circulation (with timescale of years) and the fast isentropic mixing (with timescale of days to months).

Seasonal Variations of Stratospheric Age Spectra in GEOSCCM

Li, Feng[1,2], Darryn Waugh[3], Anne R. Douglass[2], Paul A. Newman[2], Steven Pawson[2], Richard S. Stolarski[2,3], Susan E. Strahan[1,2], J. Eric Nielsen[2,4]

[1]NASA Goddard Earth Sciences Technology and Research, Greenbelt, MD, USA

[2]NASA Goddard Space Flight Center, Greenbelt, MD, USA

[3]Johns Hopkins University, Baltimore, MD, USA

[4]Science Systems and Application Inc., Lanham, MD USA

Correspondence to: Feng Li (feng.li@nasa.gov)

Abstract

The stratospheric age spectrum is the probability distribution function of the transit times since a stratospheric air parcel had last contact with a tropospheric boundary region. Previous age spectrum studies have focused on its annual mean properties. Knowledge of the age spectrum's seasonal variability is very limited. In this study, we investigate the seasonal variations of the stratospheric age spectra using the pulse tracer method in the Goddard Earth Observing System Chemistry Climate Model (GEOSCCM). The relationships between the age spectrum (also called Transit-Time Distribution, or TTD) and the Boundary Impulse Response (BIR) are reviewed and a simplified method to reconstruct seasonally varying age spectra is introduced. The age spectra in GEOSCCM have strong seasonal cycles, especially in the lowermost and lower stratosphere and the subtropical overworld. These changes reflect the seasonal evolution of the Brewer-Dobson circulation, isentropic mixing, and transport barriers. We also investigate the seasonal and interannual variations of the BIRs. Our results clearly show that computing an ensemble of seasonally dependent BIRs is necessary in order to capture the seasonal and annual mean properties of the stratospheric age spectrum.

1. Introduction

The mean age of stratospheric air is the average time for an air parcel to travel from a source region in the troposphere (or near the tropopause) to a sample region in the stratosphere [*Hall and Plumb*, 1994]. The mean age is a fundamental transport timescale that has been widely used in stratospheric transport studies, particularly in the evaluation of chemical transport models and chemistry-climate models (CCMs) [*Hall et al.,* 1999a, b; *Eyring et al.*, 2006]. However, the mean age only contains partial information of transit timescales. The complete information is included in the age spectrum, i.e., a probability distribution function of all the possible transit times since an air parcel had last contact with the tropospheric boundary source region [*Hall and Plumb*, 1994; *Waugh and Hall*, 2002]. Many studies have shown that the age spectrum is more useful than the mean age in diagnosing transport characteristics, e.g., the relative importance of different transport pathways into the lower stratosphere [*Andrews et al.*, 2001; *Bonisch et al.*, 2009], the seasonal variations of stratospheric transport [*Andrews et al.,* 1999; *Reithmeier et al.*, 2008; *Bonisch et al.*, 2009], and the horizontal recirculation rate in the tropical pipe region [*Strahan et al.*, 2009].

The age spectrum is a kind of boundary propagator. By definition, the boundary propagator $G(r,t|\Omega,t')$ is a Green's function that solves the continuity equation for the mixing ratio of a conserved and passive tracer $\chi(r,t)$ [*Hall and Plumb*, 1994]. This solution can be expressed by the following integration

$$\chi(r,t) = \int_{-\infty}^{t} \chi(\Omega,t')G(r,t\,|\,\Omega,t')dt'$$

55 where Ω is the boundary source region, r is the sample region, t' is the source time or the
56 time the tracer had last contact with Ω , and t the field time or the time the tracer is
57 sampled at r. In many cases the boundary propagator is easier to interpret if it is rewritten
58 as a function of the transit time ξ=t-t′, i.e.,

59 $$\chi(r,t) = \int_0^\infty \chi(\Omega, t-\xi) G(r,t \mid \Omega, t-\xi) d\xi$$

60 where G(r,t|Ω,t-ξ)dξ represents the mass fraction of the air parcel at r and a specific field
61 time t that was last in contact with Ω between ξ and ξ+dξ ago [*Waugh and Hall*, 2002;
62 *Holzer et al.*, 2003; *Haine et al.*, 2008]. Here G(r,t|Ω,t-ξ) is the age spectrum, and it is
63 called the Transit-Time Distribution (TTD) in tropospheric and ocean transport literatures
64 [e.g., *Holzer et al.*, 2003; *Haine et al.*, 2008]. In this paper we use TTD and age spectrum
65 interchangeably.
66
67 The age spectrum cannot be directly observed, and we rely almost solely on models to
68 compute the age spectrum. Two methods have been used to calculate the stratospheric
69 age spectrum, the pulse tracer method [*Hall et al.*, 1999b] and the trajectory method
70 [*Schoeberl et al.*, 2003]. The pulse tracer method is simpler and has been used more
71 commonly than the trajectory method. It does not need any additional software and can
72 be easily implemented. Put a pulse of a conserved and passive tracer in the boundary
73 source region Ω at a specific source time t′ and let it disperse throughout the interior area.
74 The time series of the mixing ratio of this tracer at any interior point r, which can be
75 expressed mathematically as G(r,t′+ξ|Ω,t′), represents the model's time-evolving
76 response to a delta function boundary condition. G(r,t′+ξ|Ω,t′) is called the Boundary

77 Impulse Response (BIR, *Haine et al.,* 2008). Thus the direct product of the pulse tracer
78 method is not the TTD, but the BIR. In general the BIR $G(r,t'+\xi|\Omega,t')$ is not equal to the
79 age spectrum (TTD) $G(r,t|\Omega,t-\xi)$, because the boundary propagator is a function of both
80 field time t and source time t′. However, for a stationary condition the boundary
81 propagator is only a function of the transit time ξ, i.e., for any t and t′, $G(r,t|\Omega,t-\xi) =$
82 $G(r,t'+\xi|\Omega,t')$. All the previous stratospheric pulse tracer age spectrum studies used this
83 property to compute the BIR as the TTD [*Hall and Plumb*, 1994; *Hall et al.*, 1999a, b;
84 *Schoeberl et al.*, 2005]. These studies assumed steady flow and performed a single
85 realization of the BIR as an approximation of the annul-mean or time-averaged TTD.
86
87 The traditional stratospheric pulse tracer studies have greatly improved our understanding
88 of the annual mean properties of the age spectrum [*Hall and Plumb*, 1994; *Waugh and*
89 *Hall, 2002*; *Schoeberl et al.*, 2005], but their approach has disadvantages. By assuming
90 steady flow and performing a single realization, their method cannot be used to
91 investigate the seasonality of the stratospheric age spectra. Stratospheric transport has a
92 strong seasonal cycle due to the seasonal variations of processes such as tropical
93 upwelling, subtropical jets, and polar vortices [e.g., *Chen*, 1995; *Pan et al.*, 1997;
94 *Rosenlof et al.,* 1997; *Ray et al.*, 1999; *Randel et al.*, 2001]. One would expect the
95 stratospheric age spectra to have large seasonal variations. However our knowledge of
96 the age spectrum's seasonality is very limited. To date the only work that investigated
97 the seasonal variations of stratospheric age spectra was done by *Reithmeier et al.* [2008]
98 using a trajectory method. *Reithmeier et al.* [2008] found that the age spectra in the
99 ECHAM4 general circulation model (GCM) have strong seasonal cycles, and that the

100 shapes of the age spectra change significantly with latitudes. However, there are serious
101 transport biases in ECHAM4. Specifically, the subtropical barrier is too weak and is
102 located too far away from the Equator compared to observations. These biases could be
103 related to the limitations of the version of ECHAM4 used in *Reithmeier et al.* [2008],
104 which has a very coarse horizontal (6 degrees) and vertical (only 19 levels) resolution and
105 a very low model top at 10 hPa. The model limitations and the poor transport
106 performance cast doubts on the results of *Reithmeier et al.* [2008].
107
108 Another concern about the traditional pulse tracer method is whether a single BIR is a
109 good approximation of an annual-mean age spectrum. Because in reality the stationary
110 assumption does not hold, the single BIR approach implies that the seasonality of
111 stratospheric transport has small impact on the annual mean properties of the age
112 spectrum. *Hall et al.* [1999b] found that the mean age of a single BIR agrees reasonably
113 well with the annually averaged clock tracer mean age. This was used as evidence that
114 the annual mean properties of the age spectrum could be well captured by a single BIR
115 realization. But no previous studies actually investigated the seasonal change of the BIR
116 and the differences between the TTD and the BIR in the stratosphere.
117
118 The limits of the traditional stratospheric pulse tracer method can be addressed by
119 performing an ensemble of time-dependent BIR simulations. *Holzer et al.* [2003] and
120 *Haine et al.* [2008] described in detail a straightforward method to calculate the TTDs in
121 unsteady flow using the pulse tracer. We will review their method in the next section.
122 This method requires performing a large number of BIR experiments in different seasons

123 and years to reconstruct the time-varying TTDs, and therefore it is computationally
124 expensive. We want to point out that the pulse tracer method produces a more internally
125 consistent age spectrum than the trajectory method because it uses the full and same
126 model transport operator, including processes such as parameterized mixing, diffusion,
127 and entrainment that could not be accurately represented by other methods [*Holzer et al.*,
128 2003].
129
130 In this study we investigate the seasonal variations of the age spectra in the Goddard
131 Earth Observing System Chemistry-Climate Model (GEOSCCM) using the pulse tracer
132 method. We introduce an approach to significantly reduce the computational cost for
133 calculating seasonally varying age spectra based on the method of *Holzer et al.* [2003]
134 and *Haine et al.* [2008]. Our main purpose is to understand the seasonality of the
135 stratospheric age spectra. Another purpose is to clarify the differences between the BIR
136 and the TTD. Our work broadens the usage of the pulse tracer age spectra. These results
137 will improve the understanding of the transport characteristics in the GEOSCCM, which
138 has been shown to produce realistic stratospheric transport by various diagnostics
139 [*SPARC CCMVal*, 2010]. Our results could also be used by empirical studies as guidance
140 for age spectrum's seasonal variability.
141
142 Our method for calculating the age spectra is described in Section 2. We review the
143 relationship between the TTDs and BIRs and describe how to compute TTDs and BIRs in
144 unsteady flow using a simplified version of the method of *Holzer et al.* [2003] and *Haine*
145 *et al.* [2008]. We will also briefly introduce the GEOSCCM and the simulations.

146 Seasonal variations of the TTDs are presented in Section 3. This is followed by
147 discussions of the seasonal and interannual variations of the BIRs in Section 4.
148 Discussions and summary are given in Section 5. All results presented in this paper are
149 zonally and monthly averaged and then interpolated to the isentropic coordinate.
150
151 ## 2. Method
152
153 As introduced in Section 1, the TTD and the BIR are different kind of boundary
154 propagators. They are orthogonal to each other and their relationship is illustrated in
155 Figure 1a. The contours in Figure 1a are an example of the boundary propagator at 60°N
156 and 420 K. The TTD is fixed in field time and increases toward older source time, i.e., a
157 horizontal cut through the boundary propagator map from right to left. The BIR is fixed
158 in source time and increases with field time, i.e., a vertical cut from bottom to top. For
159 unsteady flow the boundary propagator is a function of both field time t and source time
160 t' and therefore TTD and BIR are not the same (Figure 1c). Only in steady flow TTD
161 equals BIR.
162
163 The BIR can be easily computed from the pulse tracer experiment. Once the BIR is
164 obtained, the TTD can be constructed from the BIR. For steady flow, this is simple
165 because the TTD equals the BIR. And we only need to perform a single tracer
166 experiment because the age spectrum for a stationary condition has no time dependence.
167 But in reality, transport is not stationary and computing the TTD is more complicated.
168 The most direct method is to construct a complete boundary propagator map with many

successive vertical BIR sections and then a horizontal cut through the map gives the TTD (Figure 1., also see Figure 1 of *Haine et al.* [2008] and Figure 2 of *Holzer et al.* [2003]). This method requires a large number of tracer experiments, so in practice some simplifications have to be made.

We first computed twelve BIRs with twelve pulse tracers released in each month of a given model year. The method of *Hall et al.* [1999b] is followed to compute the BIR. The boundary source region is set to be the tropical lower troposphere from 10°S to 10°N and between the surface and about 800 hPa. In order to approximate the delta function boundary condition, a pulse of artificial conserved and passive tracer is uniformly released in the source region. The tracer's mixing ratio is set to an arbitrary constant value for the first month of the experiment and then held as zero through the rest of the experiment in the source region. Each experiment runs for twenty years in order to account for the long tail of the stratospheric age spectrum [*Schoeberl et al.*, 2003]. Then the time series of the tracer's mixing ratio is the BIR. Twelve pulses were released at each month of a given year and each pulse tracer produces one BIR. Figure 1b shows an example of the calculated BIRs at 60°N and 420 K as a function of source time t' and field time t. Here the source time represents when the pulses are released at the tropical surface and the field time is when the mixing ratio of the tracer is sampled in the stratosphere.

The twelve BIRs form twelve vertical sections of the boundary propagator map, but they are not enough to reconstruct the TTDs. For a 20-year long TTD, a total of 240 pulse

192 experiments are needed. In practice it is not possible to run such a large number of
193 experiments with the GEOSCCM. So we make an initial assumption that the BIR's
194 interannual variability is sufficiently small compared to its seasonal variability that we
195 can ignore age spectrum's interannual variations for the purpose of this study. We will
196 show in section 4 that this is a reasonable assumption in GEOSCCM. Under this
197 assumption, we construct the boundary propagator map by simply repeating the 12 BIRs
198 every year for 20 years and shifting the source time accordingly, i.e., let $G(r,t'+\xi|\Omega,t') =$
199 $G(r,t'+\xi+n\times12|\Omega,t'+n\times12)$, where t' = Jan, Feb,...Dec represents the source time of the
200 pulse tracer experiments, and n = 1, 20 are the repeating years. We then obtain the TTDs
201 as horizontal cuts through the map (Figure 1a). In the next section we show evidence that
202 our method is valid in a climatological mean sense, i.e., our calculation captures very
203 well the seasonality of the climatological mean.
204
205 The pulse experiments were performed in a transient simulation using the GEOSCCM
206 Version 2. GEOSCCM Version 2 is an update from GEOSCCM version 1 [*Pawson et*
207 *al.*, 2008]. It couples the GEOS5-GCM [*Reineker et al.*, 2008] with a comprehensive
208 stratospheric chemistry package [*Douglass et al.*, 1996]. The model has 72 vertical levels
209 with a top level at 1 Pa. The simulation was carried out on a horizontal resolution of 2^{o}
210 latitude by 2.5^{o} longitude. The twelve pulses were released in each month of model year
211 2000 and ran for 20 years to 2019, where the model year represents the conditions of the
212 external forcings. The simulation was forced with IPCC (2001) greenhouse gas (GHG)
213 scenario A1b and WMO (2007) ozone depleting substance scenario A1. The sea surface
214 temperature and sea ice contents were taken from an NCAR Community Climate System

215 Model 3.0 run in the A1b GHG scenario. The solar forcing was held constant in the
216 experiments.
217
218 Results from GEOSCCM Version 2 have been extensively analyzed and evaluated using
219 observation-based process-oriented diagnostics along with other CCMs in the SPARC
220 CCMVal-2 project [*SPARC CCMVal*, 2010]. Overall GEOSCCM performs well in terms
221 of the stratospheric dynamical and thermal structure, trace gas distributions, and their
222 decadal changes in the recent past. GEOSCCM has quite realistic transport
223 characteristics in the stratosphere. The tropical ascent rates, the lower stratospheric
224 mixing rates, and the mean age compare well to observations. GEOSCCM has the best
225 performance in mean age among all the CCMs that participated in the CCMVal-2. But
226 GEOSCCM has a somewhat stronger subtropical barrier in the middle stratosphere and a
227 stronger Antarctic polar vortex barrier than observed.
228
229 **3. Seasonal Variations of the Transient Time Distribution**
230
231 Three parameters that characterize aspects of the age spectra are the modal age $\tau_M(r,t)$,
232 the mean age $\Gamma(r,t)$, and the width $\Delta(r,t)$ [*Waugh and Hall*, 2002]. The modal age is the
233 most probable transit time, corresponding to the time of the spectral peak. The mean age
234 is the first moment of the age spectrum $\Gamma(r,t) = \int_0^\infty \xi G(r,t \mid \Omega, t-\xi) d\xi$ and represents the
235 average transit time. The width is related to the second moment of the age spectrum
236 $\Delta(r \mid t) = \sqrt{\frac{1}{2}\int_0^\infty (\xi - \Gamma(r \mid t))^2 G(r,t \mid \Omega, t-\xi) d\xi}$, which is a measure of the spread of the

237 spectrum. Among the three parameters, only the mean age can be derived from
238 measurements and its seasonal variability has been studied before [*Andrews et al.*, 1999;
239 *Reithmeier et al.*, 2008; *Bonisch et al.*, 2009]. Here we first show the seasonal variations
240 of the mean age.
241
242 Figure 2 shows the mean age (contour) and its differences from the annually averaged
243 mean age (color) as functions of latitude and potential temperature at two month
244 intervals. The mean age has significant seasonal variations and these variations change
245 with latitude and height (also see Figures 5a, 5d, and 5g which show the seasonal
246 evolution of the mean age at the 360 K, 420 K, and 550 K isentropic surface). In the
247 extratropical lower stratosphere (poleward of about 30° degrees latitude and below about
248 the 500 K isentropic surface), the mean age has a strong annual cycle with the youngest
249 air in summer and early fall and the oldest air in winter and early spring. Large seasonal
250 change is also found in the subtropical lower stratosphere (between 10° and 30° degrees
251 latitude and below about 450 K). Its magnitude is smaller than that in the extratropics in
252 absolute value, but is comparable in relative change, which is up to 40% different from
253 the annual-mean value. In winter/early spring and summer/early fall, the seasonal cycle
254 in the subtropical lower stratosphere is nearly out-of-phase with that in the extratropics.
255 In the middle and upper stratosphere above about 500 K the seasonal variability of the
256 mean age is generally smaller than that in the lower stratosphere, and the largest seasonal
257 variations are found in the subtropics.
258

259 Before discussing the seasonal variations of the TTDs in more detail, we conduct a
260 consistency check within the model by comparing the TTD mean age and its seasonal
261 cycle with the model clock tracer mean age. The clock tracer is a linearly increasing
262 tracer whose source region is at the global surface. For the clock tracer, the mean age is
263 simply calculated as the time lag between the stratospheric sample region and the
264 reference region, defined here as the tropical surface in order to be consistent with the
265 pulse tracer experiment. This consistency check can determine whether our calculated
266 TTD mean age is correct and whether it is worth investigating further into the seasonality
267 of the TTDs. Figure 3 shows the climatology of the monthly clock tracer mean age
268 distribution. Comparing Figure 3 with Figure 2 clearly shows that the clock tracer and
269 age spectrum have almost exactly the same mean age distribution and seasonal variations.
270 Small differences are found in the tropopause region. It appears that the clock tracer
271 mean age is a bit younger and its seasonal cycle is stronger than the age spectrum mean
272 age in the extratropical tropopause region. Nevertheless, given the completely different
273 methodology in the TTD and the clock tracer, the overall very similar mean age seasonal
274 evolution in these two methods provides convincing evidence that our calculation of the
275 TTD is valid, in the sense it represents very well the climatological seasonal variations of
276 the age spectra.
277
278 The model simulated mean age seasonal variations agree well with the small number of
279 observational studies that have been published to date. *Bonisch et al.* [2009] investigated
280 this topic with mean age derived from in-situ measurements of SF_6 and CO_2 during the
281 SPURT aircraft campaigns that were carried out in the upper troposphere/lower

282 stratosphere in the extratropics over Europe. They found that in the lowermost
283 stratosphere bounded by the tropopause and the 380 K isentropic surface, the oldest air (>
284 3 years) was observed in April and the youngest air (< 1 year) was observed in October.
285 Our model results are consistent with *Bonisch et al.* [2009], although the oldest air occurs
286 in March and the youngest air occurs in September in our model calculations (note there
287 are no March and September data in *Bonisch et al.*, 2009). This agreement gives us more
288 confidence in our calculations.
289
290 The seasonal change of the mean age reflects the seasonality of stratospheric transport.
291 In a simplified view, the stratospheric transport is controlled by the integrated effects of
292 the slow Brewer-Dobson circulation (with timescale of years) and the relatively fast
293 isentropic mixing (with timescale of weeks to months). The Brewer-Dobson circulation
294 is strongest in NH winter and weakest in NH summer [*Rosenlof*, 1995]. The seasonal
295 variations of isentropic mixing are controlled by the seasonal evolution of the mixing
296 barriers. There are three mixing barriers, which can be identified by the locations of the
297 strongest gradients in Figure 2 (indicated by symbol X). The polar barrier, located at the
298 edge of the polar vortex in winter and early spring, suppresses mixing between the polar
299 old air and midlatitude young air. The subtropical barrier isolates the tropical pipe from
300 the surf zone in the overworld and it is strongest in late winter/early spring and weakest
301 in late summer/early fall. The tropospheric jet or tropopause barrier significantly limits
302 cross-tropopause mixing between the tropical upper troposphere and the midlatitude
303 lowermost stratosphere in winter. The seasonal variations of the mean age are
304 determined by the relative importance of these processes.

305

306 The seasonal cycle of the mean age in the extratropical lowermost stratosphere (between
307 about the tropopause and the 380 K isentropic surface) indicates that the fast isentropic
308 mixing between the tropical upper troposphere or Tropical Tropopause Layer (TTL) and
309 the midlatitude lowermost stratosphere is most important in summer/early fall and least
310 important in winter/early spring [*Bonisch et al.*, 2009]. This is consistent with the
311 seasonal cycle of the tropical jet and tropopause barrier [*Chen*, 1995; *Pan et al.*, 1997].
312 The tropospheric jet is weak and the tropopause is high during the summer/early fall
313 (Figures 4a and 4b), and the cross-tropopause isentropic mixing is strong. In winter/early
314 spring the strong tropospheric jet and low tropopause height significantly suppress the
315 cross-tropopause mixing. The strong wintertime and weak summertime Brewer-Dobson
316 circulation descent might also play a role in determining the seasonal change of the mean
317 age in the lowermost stratosphere.
318

319 A very similar cycle is found in the extratropical lower stratosphere between about the
320 380 K and 500 K isentropic surface. Again this suggests that isentropic mixing has the
321 largest impact and Brewer-Dobson circulation descent has the smallest impact in
322 summer/early fall. In the polar stratosphere the seasonal evolution of the Brewer-Dobson
323 circulation and the polar barrier determine the seasonal change of the mean age. In
324 winter the strong descent brings old air to the polar region from higher altitudes. The
325 polar barrier prohibits mixing between the old polar air and the young midlatitude air
326 throughout the winter, resulting in the oldest air in the spring polar region. In summer

and early fall, mixing with the younger midlatitude air and weak descent result in the youngest polar air.

One interesting feature is the near opposite phase of the seasonal cycle of the mean age in the subtropical and midlatitude lower stratosphere below about the 450 K isentropic surface. This feature is most clearly seen in the NH in January, March and July, September in Figure 2 (also see Figures 5a and 5d). The seasonal change of the subtropical lower stratospheric mean age cannot be explained by that of the tropical upwelling. The strongest upwelling occurs in the subtropics of the summer hemisphere (Figure 4c), but the oldest subtropical air is found in the summer hemisphere. One possible explanation is that the opposite phase reflects the seasonal cycle of isentropic mixing in this region. The strong mixing in summer/early fall between the subtropics and midlatitudes leads to anomalously old subtropical air and young midlatitude air. And the weak isentropic mixing in winter/early fall leads to anomalously young subtropical air and old midlatitude air. It should be noted, however, that there are no observational studies on the mean age's seasonal variations in the subtropical lower stratosphere. Thus this model feature needs to be verified by observations of the mean age.

We also note the phase of the seasonal cycle of the subtropical mean age changes above the 450 K isentropic surface, which is most clearly seen in winter/early spring and summer/early fall. This suggests the base of the tropical pipe is located at about 450 K, consistent with observations [*Rosenlof et al.*, 1997]. The edge of the lower tropical pipe moves toward the equator in late winter/early spring and brings old air to the subtropical

350 lower stratosphere above 450 K. It moves away from the equator in late summer/early
351 fall and the subtropical lower stratosphere is filled with more young tropical air.
352
353 The age spectra provide additional information on transit timescales. Figure 5 shows the
354 seasonal evolution of the modal age, width and the mean age at the 360, 420, and 550 K
355 isentropic surfaces. Outside the Tropics the 360 K isentropic surface represents the
356 lowermost stratosphere. The 420 K isentrope is used to represent the tropically
357 controlled transition region, which is bounded between approximately the 380 K and 450
358 K isentropic surfaces [*Rosenlof et al.*, 1997]. And the 550 K is chosen to represent the
359 overworld. The width is an important age spectrum parameter [*Hall and Plumb*, 1994].
360 Physically it is a measure of the strength of the recirculation [*Strahan et al.*, 2009]. A
361 stronger recirculation leads to a wider width, longer tail, and older mean of the spectra.
362 Thus it is not surprising that the width has almost the same seasonal variations as the
363 mean age.
364
365 The modal age represents the timescale of the most common path. Its seasonal change is
366 similar to that of the mean age, but the modal age change is more abrupt. At 360 K the
367 modal age is 1 month equatorward of 30°N and S for all seasons. But at high latitudes
368 the modal age is younger in summer than other seasons. This summer shortcut can also
369 be clearly seen at 420K, especially in the NH. For instance, it takes only two months to
370 transport the spectral peak from the TTL to the NH high latitudes during Jun-Aug. But
371 this fast path is shut off during winter/early spring, as illustrated by the strong gradients
372 in the sub-polar latitudes. These large gradients, also seen in the mean age, show the

373 change of the relative importance of the fast isentropic mixing and the slow Brewer-
374 Dobson circulation descent in winter/early spring due to the combined effect of the strong
375 wintertime adiabatic descent and the polar barrier. The modal age at 550 K shows very
376 dramatic seasonal variations at high latitudes. Interestingly the strongest gradient in the
377 mean age occurs in the subtropics, representing the impact of the subtropical barrier that
378 isolates the tropical pipe from the surf zone. However, the subtropical barrier is not clear
379 in the modal age.
380
381 We now examine the seasonal cycle of the age spectra at some chosen latitudes at the
382 360, 420, and 550 K isentropic surfaces. At 360 K and 20°N a narrow spectral peak at 1
383 month characterizes the age spectra (Figure 6). The modal ages are the same for all
384 seasons, but the width is wider in summer than in winter. At 46°N, the strongest spectral
385 peaks and the youngest peak value (1 month) occur in August and September. The
386 weakest peaks (about half that in fall) with the oldest peak values (3 months) occur in
387 March and April, suggesting that the fast pathway evident during the summer is
388 suppressed during the winter. Almost exactly the same seasonal variations are found at
389 high latitudes. At 80°N, the fall age spectra have the youngest mean age and the
390 strongest spectral peak. Their modal age of 4-5 months indicates that the spectral peaks
391 leave the source region in late spring/early summer. The spring spectra have the oldest
392 mean and model age, and their spectral peaks are traced back to fall of the previous year.
393 These results are consistent with the wintertime tropospheric jet barrier in the lowermost
394 stratosphere. The SH age spectra have very similar seasonal variability as their NH
395 counterparts.

396

397 The overall seasonal change in the age spectra at the 420 K isentropic surface (Figure 7)
398 is similar to that at 360 K. One feature in the 420 K age spectra not seen in the
399 lowermost stratosphere is the large change in the modal age at high latitudes (also see
400 Figure 5e). For instance at 80°S the modal age changes dramatically from about 0.75
401 year in the February spectrum to about 4 years in the November spectrum. The sharp
402 jump in the winter/early spring modal age is associated with significant changes in the
403 spectral shape. For example, the February and March spectra at 80°N have three
404 comparable peaks with transit time of about 1.2, 2.7 and 3.7 years, respectively. The
405 second peak is a bit higher than the other two and that is the modal age by definition.
406 Apparently the modal age is not a very useful parameter to characterize the spectral shape
407 for this kind of spectrum. Note even the first peak is much older than the 0.5 year modal
408 age of the summer spectra. Also the magnitude of the February-March peaks is about ¼
409 of the July-August spectra. We interpret this as the seasonal change of the dominant
410 pathway at high latitudes. In summer/early fall, isentropic mixing brings young TTL air
411 directly to the polar region. In winter/spring, slow descent from high altitude dominates.
412

413 The 550 K age spectra also show large jumps in modal age at high latitudes (Figure 8).
414 The modal ages of the winter/spring spectra are much older (up to two times) than those
415 of the summer spectra, but their magnitudes are stronger. This suggests that mixing
416 between middle and high latitudes in summer, which is weak because of the summer
417 stratospheric easterlies, leads to a younger although weaker spectral peak in the polar
418 region. In winter/spring the mixing is prohibited and the spectral peaks represent solely

419 the descent of the Brewer-Dobson circulation. The younger and weaker summer spectral
420 peak is a unique feature in the overworld high latitudes and it explains the relatively
421 small mean age seasonal cycle in this region.
422
423 The change of the spectral shape from a single peak at low and middle latitudes to
424 multiple peaks at high latitudes was first reported by *Reithmeier et al.* [2008], who
425 calculated age spectra in the ECHAM4 GCM using the Lagrangian trajectory method. A
426 major focus of *Reithmeier et al.* [2008] was to understand what causes the high latitudes
427 multiple spectral peaks, which are 1 year apart and independent of height. They argued
428 that these multi-modal polar spectra are caused by two processes: the seasonality of the
429 tropical upwelling that generates single mode spectra at midlatitudes, and the
430 summertime mixing between the polar and midlatitude air that leads to a superposition of
431 the midlatitude single mode spectra with the polar spectra once a year and generates
432 multiple annual peaks.
433
434 Although our TTDs show multiple peaks similar to those in *Reithmeier et al.* [2008],
435 there are some differences. Figure 9 shows the March and September age spectra at 80°N
436 and S at 420 K. The starts of the age spectra are shifted such that the x-axis reflects the
437 season of the source time. The age spectra are plotted in the logarithmic scale to
438 highlight the tail region. In both the NH and SH high latitudes, the annually repeating
439 peaks last contacted the tropical surface during their respective summer season. This is
440 not the case in *Reithmeier et al.* [2008] (see their Figures 5 and 9). These annual peaks
441 are very clear in the tail region, suggesting they are caused by the annual cycle of the

442 recirculation into the polar stratosphere. Our results indicate that air parcels leaving the
443 tropical surface in summer have a larger chance to be re-circulated into the polar
444 stratosphere. Apparently the annual cycle of the Brewer-Dobson circulation and polar
445 vortex barrier determine the annual cycle of the recirculation into the polar region, but the
446 mechanism is not clear.
447
448 The tails of the age spectra, defined here as regions with transit time older than 4 years,
449 decay exponentially with time. Thus the tails can be approximated by an exponentially
450 decaying mode $\Psi_0(r,t)\exp(-\frac{\xi}{\tau_0})$ (straight solid lines in Figure 9). This decay rate τ_0 is
451 the eigentime of the lowest mode of the age spectra [*Hall et al.*, 1999a; *Ehhalt et al.*,
452 2004]. It is a fundamental stratospheric transport diagnostic and remains nearly constant
453 in different seasons and locations (2.77 years in GEOSCCM). Of course this does not
454 mean that the tails are not seasonal dependent, because $\Psi_0(r,t)$ changes with season and
455 location.
456

457 4. Seasonal and Interannual Variations of the Boundary Impulse
458 Response

459
460 A concern about the traditional pulse tracer approach is that it uses only a single BIR
461 realization to approximate the annual-mean TTD. *Haine et al.* [2008] showed
462 theoretically that the statistical properties of an ensemble mean of the TTDs are
463 equivalent to those of an ensemble mean of the BIRs in unsteady flow. We have
464 compared the annual-mean TTDs and BIRs in our model simulations and have found

465 they are nearly identical (not shown). This means if the seasonality of the BIR is small, a
466 single BIR realization could be a good representation of an annual-mean TTD.
467
468 Our simulations show significant seasonal variations in the BIR. In order to illustration
469 the BIR's seasonality, Figure 10 plots the seasonal evolution of the BIR mean age, modal
470 age, and width at 420 K. The seasonal change is small in the tropics, but becomes
471 significant at high latitudes. For example, in the NH polar region, the mean age of the
472 winter released BIR (about 2.75 years) is about 25% younger than the mean age of the
473 summer released BIR (3.5 years). And the modal age of the spring BIR (5 months) is
474 only half of the summer value (10 months). Cleary, the annual-mean properties of the
475 age spectrum cannot be well captured by a single BIR in areas of large BIR seasonality
476 such as the polar region.
477
478 We also want to emphasize that the seasonal change of the BIR, which is based on the
479 source time, could be very different from the seasonal change of the TTD that is based on
480 the field time. Our model results show that both the phase and magnitude of the BIR's
481 seasonal cycle are different from those of the TTD's (compare Figure 10 with Figures 5d-
482 5f). One striking difference is the shift of the phase in the extratropics between the BIR
483 and TTD. The summer-released BIRs have the oldest mean age, modal age and the
484 largest width, which is nearly out of phase with the TTDs whose youngest mean and
485 modal age, and smallest width occur in the late summer/early fall. It can be also clearly
486 seen that the seasonal change of the BIR is much smaller than that in TTD.
487

488 In order to help to understand the different seasonality in the BIR and the TTD the
489 seasonal evolution of the BIRs at 80°N and 420 K is plotted in Figure 11. This is similar
490 to Figure 1b, but only the first two years of the BIRs are shown. The most interesting
491 feature is that the modal ages of the BIRs are seasonally locked to the summer field time.
492 No matter when the pulse is released, its peak always reaches high latitudes during Jun-
493 Aug. It takes about 6 months for the peaks of the winter-released pulse to arrive 80°N.
494 The transport of summer-released BIRs into the polar lower stratosphere is strongly
495 suppressed in winter and early spring by the vortex barrier. They do not penetrate into
496 the high latitudes until the breakup of the polar vortex in late spring. This leads to the
497 oldest and weakest spectral peaks, meaning that the summer-released BIRs have the
498 smallest fraction of young air and thus oldest mean age. Furthermore, the summer/early
499 fall peaks and winter/early spring valleys with respect to the field time means that the
500 TTDs, which are horizontal cuts from right to left through the boundary propagator map,
501 have the youngest mean age in summer/late fall and oldest mean age in winter/early
502 spring (see Figure 7).
503
504 We made an initial assumption in this study that the BIR's interannual variations are
505 smaller than its seasonal variations. We performed eight additional pulse experiments to
506 verify that this assumption is valid. The eight pulses were released respectively in
507 January and July in years 2001 to 2004. Since we already have the January and July BIR
508 for year 2000, a total of five January-released and five July-released BIRs for 2000-2004
509 were obtained. The mean and standard deviations of the five January (black) and July
510 (red) BIRs at some chosen locations in the NH are shown in Figure 12. The SH has very

511 similar features and is not shown. In the subtropical lower stratosphere (20°N at 360 K
512 and 420K) the interannual variations are very small such that the lines representing the
513 standard deviation almost overlap with the mean BIR. In the midlatitude lower
514 stratosphere the magnitude of the spectral peaks shows some interannual variations.
515 Considerable interannual changes are found in the 550 K extratropics and polar lower
516 stratosphere. Nevertheless, the seasonal differences between the January and July BIRs
517 clearly stand out.
518
519 We have already shown that the TTD mean age agrees very well with the clock tracer
520 mean age (Figures 2 and 3). We compared closely the mean age's seasonal change in the
521 polar region where relatively large interannual variations occur, and found excellent
522 agreements between the TTD and clock tracer mean age. These results suggest that the
523 interannual variability of the BIR has only small impact on our calculations of the TTDs.
524
525 **5. Discussion and Summary**
526
527 The seasonal variations of the stratospheric TTDs are investigated in this study using the
528 pulse tracer method in GEOSCCM. We have found that the TTDs have significant
529 seasonal variations throughout the stratosphere. The largest seasonal changes occur in
530 the lowermost and lower stratosphere and the subtropical overworld. Up to 40%
531 differences between the individual month and annually averaged mean age are commonly
532 found in these regions. The modal ages and spectral shapes demonstrate even bigger
533 changes in the polar stratosphere. The seasonal variations of the TTDs reflect the

seasonal evolution and relative importance of the slow Brewer-Dobson circulation and the fast isentropic mixing.

The differences between the TTD and the BIR are known in tropospheric and ocean transport studies [*Holzer et al.*, 2003; *Haine et al.*, 2008], but the BIR is often used as the TTD in stratospheric transport [*Hall and Plumb*, 1994; *Hall et al.*, 1999a, b; *Schoeberl et al.*, 2005]. These studies perform a single pulse tracer experiment and the resultant BIR is used as an approximation of the time-averaged TTD. Here we show that the BIRs have significant seasonal variations. Thus it is problematic to use a single BIR realization to represent the annually averaged TTDs. Our model results also show that the phase and magnitude of the BIR's seasonal cycle are different from those of the TTD's. Clearly it is misleading to use BIRs to study the seasonality of the TTDs. On the other hand, *Haine et al.* [2008] showed theoretically that an ensemble-averaged BIR is equivalent to an ensemble-averaged TTD. This is confirmed by the nearly identical annually averaged BIR and TTD in our results (not shown). In summary, computing an ensemble of BIRs is needed in order to investigate either the seasonality or the annual-mean properties of the TTDs.

Several studies have used empirical age spectra to investigate stratospheric transport [*Andrews et al.*, 1999, 2001; *Bonisch et al.*, 2009]. They assumed an analytic solution for the age spectra and used in-situ trace gas measurements to constrain the empirical parameters. *Andrews et al.* [2001] proposed a bimodal spectral shape with two distinct peaks to represent respectively the fast quasi-horizontal mixing and slow Brewer-Dobson

557 circulation in the NH midlatitude lower stratosphere. *Bonisch et al.* [2009] adopted this
558 bimodal concept and made important revision that the superposition of the two modes
559 does not necessarily lead to two distinct spectral peaks. The age spectra in GEOSCCM
560 show a single peak in this region (see Figures 6 and 7), which does not support the
561 bimodal shape of *Andrews et al.* [2001]. Our results appear to be consistent with the
562 conceptual model of *Bonisch et al.* [2009]. However, *Bonisch et al.* [2009] concentrated
563 on the mean age and did not present the seasonal evolution of their empirical age spectra.
564 Therefore we could not make direct comparisons with *Bonisch et al.* [2009]. We do find
565 multi-modal spectral shapes at high latitudes, but the multiple spectral peaks are due to
566 the annual cycle of air recirculation. As pointed out by *Reithmeier et al.* [2008], it is very
567 challenging to apply this multi-modal spectral shape in empirical studies.
568
569 An importance implication of our results is on the long-term changes in the mean age.
570 Chemistry climate models consistently simulate a decrease of the stratospheric mean age
571 in the recent past and in the 21st century at a rate about 2-3%/decade [e.g., *Garcia and*
572 *Randel*, 2008; *Oman et al.,* 2009]. The decrease in the mean age is consistent with the
573 acceleration of the Brewer-Dobson circulation [*Austin and Li,* 2006; *Li et al.*, 2008].
574 However, the acceleration of the Brewer-Dobson circulation is directly related to the
575 decrease of the modal age, not the mean age [*Strahan et al.*, 2009]. Of course a younger
576 modal age could result in a younger mean age, but other processes, such as a weakening
577 of recirculation and/or a decrease in the long-term decay timescale, could also contribute
578 to the decrease of the mean age. We will investigate the long-term changes in the
579 stratospheric age spectra in a warming climate in a separate study.

Acknowledgements.

This work is supported by NASA's Modeling, Analysis and Prediction program. We thank Laura Pan for very helpful discussions. Computational resources for this work were provided by NASA's High-Performance Computing through the generous award of computing time at NASA Ames Research Center.

588 **References**

589

590 Andrews, A. E., K. A. Boering, B. C. Daube, S. C. Wofsy, E. J. Hintsa, E. M. Weinstock,
591 and T. P. Bui (1999), Empirical age spectra for the lower tropical stratosphere from in
592 situ observations of CO_2: Implications for stratospheric transport, *J. Geophys. Res., 104*,
593 26,581– 26,595.

594

595 Andrews, A. E., K. A. Boering, S. C. Wofsy, B. C. Daube, D. B. Jones, S. Alex, M.
596 Loewenstein, J. R. Podolske, and S. E. Strahan (2001), Mean ages of stratospheric air
597 derived from in situ observations of CO_2, CH_4, and N_2O, *J. Geophys. Res., 106*, 32,295–
598 32,314.

599

600 Austin, J., and F. Li (2006), On the relationship between the strength of the Brewer-
601 Dobson circulation and the age of stratospheric air, *Geophys. Res. Lett., 33*, L17807,
602 doi:10.1029/2006GL026867.

603

604 Boering, K. A., S. C. Wofsy, B. C. Daube, H. R. Schneider, M. Loewenstein, J. R.
605 Podolske, and T. J. Conway (1996), Stratospheric mean ages and transport rates from
606 observations of carbon dioxide and nitrous oxide, *Science*, 274, 1340–1343.

607

608 Bonisch, H., A. Engel, J. Curtius, T. Birner, and P. Hoor (2009), Quantifying transport
609 into the lowermost stratosphere using simultaneous in-situ measurements of SF_6 and CO_2,
610 *Atmos. Chem. Phys. 9*, 5905-5919.

611

612 Chen, P. (1995), Isentropic cross-tropopause mass exchange in the extratropics, *J.*
613 *Geophys. Res.*, 100, 16661-16673.

614

615 Douglass, A. R., C. J. Weaver, R. B. Rood, and L. Coy (1996), A three dimensional
616 simulation of the ozone annual cycle using winds from a data assimilation system, *J.*
617 *Geophys. Res.*, 101(D1), 1463–1474.

618

619 Ehhalt, D. H., F. Rohrer, S. Schauffler, and M. Prather (2004), On the decay of
620 stratospheric pollutants: Diagnosing the longest-lived eigenmode, *J. Geophys. Res.*, 109,
621 D08102, doi:10.1029/2003JD004029.

622

623 Eyring, V., et al. (2006), Assessment of temperature, trace species, and ozone in
624 chemistry-climate model simulations of the recent past, *J. Geophys. Res., 111*, D22308,
625 doi:10.1029/2006JD007327.

626

627 Garcia, R. R., and W. Randel (2008), Acceleration of the Brewer–Dobson circulation due
628 to increases in greenhouse gases. *J. Atmos. Sci.*, 65, 2731–2739.

629

630 Haine, T. W. N., H. Zhang, D. W. Waugh, and M. Holzer (2008), On transit-time
631 distributions in unsteady circulation models, *Ocean Modelling*, 21, 35-45.

632

633 Hall, T. M., and R. A. Plumb (1994), Age as a diagnostic of stratospheric transport, *J.*
634 *Geophys. Res., 99*, 1059-1070.
635
636 Hall, T. H., D. J. Wuebbles, K. A. Boering, R. S. Eckman, J. Lerner, R. A. Plumb, D. H.
637 Rind, C. P. Rinsland, D. W. Waugh, and C.-F. Wei (1999a), Transport experiments, in
638 Models and Measurements Intercomparison II, edited by J. H. Park et al., Rep.
639 NASA/TM-1999-20,9554, chap. 2, pp. 110–189, NASA, Hampton, Va.
640
641 Hall, T. M., D. W. Waugh, K. A. Boering, and R. A. Plumb (1999b), Evaluation of
642 transport in stratospheric models, *J. Geophys. Res., 104*, 18815-18839.
643
644 Holzer, M., I. G. McKendry, and D. A. Jaffe (2003), Springtime trans-Pacific
645 atmospheric transport from east Asia: A transit-time probability density function
646 approach, *J. Geophys. Res.*, 108(D22), 4708, doi:10.1029/2003JD003558.
647
648 Li, F., J. Austin, and J. Wilson (2008), The strength of the Brewer–Dobson circulation in
649 a changing climate: Coupled chemistry–climate model simulations. *J. Climate*, 21, 40–
650 57.
651
652 Oman, L., D. W. Waugh, S. Pawson, R. S. Stolarski, and P. A. Newman (2009), On the
653 influence of anthropogenic forcings on changes in the stratospheric mean age, *J.*
654 *Geophys. Res.*, 114, D03105, doi:10.1029/2008JD010378.
655

656 Pan, L., S. Solomon, W. Randel, J.-F. Lamarque, P. Hess, J. Gille, E.-W. Chiou, and M.
657 P. McCormick (1997), Hemispheric asymmetries and seasonal variations of the
658 lowermost stratospheric water vapor and ozone derived from SAGE II data, *J. Geophys.*
659 *Res.*, 102, 28177-28184.
660
661 Pawson, S., R. S. Stolarski, A. R. Douglass, P. A. Newman, J. E. Nielsen, S. M. Frith,
662 and M. L. Gupta (2008), Goddard Earth Observing System chemistry climate model
663 simulations of stratosphere ozone temperature coupling between 1950 and 2005, *J.*
664 *Geophys. Res.*, 113(D12), D12103, doi:10.1029/2007JD009511.
665
666 Randel, J. W., F. Wu, A. Gettelman, J. M. Russell III, J. M. Zawodnya, and S. J. Oltmans
667 (2001), Seasonal variation of water vapor in the lower stratosphere observed in Halogen
668 Occultation Experiment data, *J. Geophys. Res.,* 106, 14313-14325.
669
670 Ray, E. A., F. L. Moore, J. W. Elkins, G. S. Dutton, D. W. Fahey, H. Vomel, S. J.
671 Oltmans, and K. H. Rosenlof (1999), Transport into the Northern Hemisphere lowermost
672 stratosphere revealed by in situ tracer measurements, *J. Geophys. Res.*, 104, 26565-
673 26580.
674
675 Reithmeier, C., R. Sausen, and V. Grewe (2008), Investigating lower stratospheric model
676 transport: Lagrangian calculation of mean age and age spectra in the GCM ECHAM4,
677 *Clim. Dyn.*, 30, 225-238.
678

679 Rienecker, M. M., et al. (2008), The GEOS-5 data assimilation system— Documentation
680 of versions 5.0.1, 5.1.0, and 5.2.0, in Technical Report Series on Global Modeling and
681 Data Assimilation, NASA Tech. Memo., TM-2008-10460627.
682
683 Rosenlof, K. H. (1995), Seasonal cycle of the residual mean meridional circulation in the
684 stratosphere, *J. Geophys. Res.*, 100 (D3), 5173-5191.
685
686 Rosenlof, K. H., A. F. Tuck, K. K. Kelly, J. M. Russell III, and M. P. McCormick (1997),
687 Hemispheric asymmetries in water vapor and inferences about transport in the lower
688 stratosphere, *J. Geophys. Res.*, 102, 13213-13234.
689
690 Schoeberl, M. R., A. R. Douglass, Z. Zhu, and S. Pawson (2003), A comparison of the
691 lower stratospheric age spectra derived from a general circulation model and two data
692 assimilation systems, *J. Geophys. Res., 108*(D3), 4113, doi:10.1029/2002JD002652.
693
694 Schoeberl, M. R., A. R. Douglass, B. Polansky, C. Boone, K. A. Walker, and P. Bernath
695 (2005), Estimation of stratospheric age spectrum from chemical tracers, *J. Geophys. Res.*,
696 *110*, D21303, doi:10.1029/2005JD006125.
697
698 Spackman, J. R., E. M. Weinstock, J. G. Anderson, D. F. Hurst, H.-J. Jost, and S. M.
699 Schauffler (2007), Aircraft observations of rapid meridional transport from the tropical
700 tropopause layer into the lowermost stratosphere: Implications for midlatitude ozone, *J.*
701 *Geophys. Res., 112*, D12308, doi:10.1029/2006JD007618.

SPARC CCMVal (2010), SPARC CCMVal Report on the Evaluation of Chemistry-Climate Models, V. Eyring, T. G. Shepherd, D. W. Waugh (Eds.), SPARC Report No. 5, WCRP-X, WMO/TD-No. X, http://www.atmosp.physics.utoronto.ca/SPARC.

Strahan, S. E., M. R. Schoeberl, and S. D. Steenrod (2009), The impact of tropical recirculation of polar composition, *Atmos. Chem. Phys., 9*, 2471-2480.

Waugh, D. W., and T. M. Hall (2002), Age of stratospheric air: Theory, observations, and models, *Rev. Geophys., 40*(4), 1010.doi:10.1029/2009RG000101.

Figure Captions

Figure1: Illustration of the relationship between the Transit-Time Distribution (TTD) and Boundary Impulse Response (BIR). Panel (a) is a boundary propagator map at 60°N and 420 K. This map is constructed from 252 vertical slices. Each vertical slice is a BIR, which is fixed in source time and increases with field time. The TTD is fixed in field time and increases towards older source time, i.e., a horizontal cut from right to left through the boundary propagator map. An example of the BIR and TTD is shown in panel (c). When constructing the boundary propagator map (a), we do not calculate all the 252 BIRs. Instead we only calculate 12 BIRs with source time in each month of a given year. These 12 BIR realizations (shown in panel b and in the black rectangle in panel a) are then repeated every year for 20 years to form the boundary propagator map.

Figure 2: Distribution of the TTD mean age (contour) and its difference from the annually averaged mean age (color) at two month intervals. The contour interval is 0.5 yr. The red line is the tropopause. The symbol X in the January panel indicates the location of the transport barriers.

Figure 3: Same as Figure 2, but for the climatological mean (2000-2019) clock tracer mean age.

Figure 4: Seasonal cycle of (a) the zonal wind at 360 K; (b) the tropopause height; (c) the residual vertical velocity at 360 K.

735

736 Figure 5: Seasonal evolution of the TTD mean age, modal age, and width at 360, 420 and
737 550 K. The contour interval is 0.25 year for the mean age and 0.2 yr for the width. The
738 unit of the modal age is month and variable contour intervals are used in different levels:
739 1 month at 360 K, 2 months (modal age < 1 yr) and 4 months (modal age > 1 yr) at 420
740 K, and 4 months at 550 K.

741

742 Figure 6: Seasonal cycle of the TTDs at 20°, 46°, and 80° latitude north and south at 360
743 K. The dotted line is the modal age and the solid line is the mean age. The colors in each
744 panel are normalized by the maximum PDF shown in the caption.

745

746 Figure 7: Same as Figure 6, but for 420 K.

747

748 Figure 8: Same as Figure 6, but for 550 K.

749

750 Figure 9: The March (black) and September (red) TTDs at 80°N and S at 420 K. The
751 starts of the age spectra are shifted (indicated by the thin dash lines) so that the x-axis
752 represents the season of the source time. The vertical dotted lines correspond to January
753 in source time.

754

755 Figure 10: Seasonal evolution of the BIR mean age, modal age and width at 420 K. The
756 contour interval is 0.25 year for the mean age and 0.2 year for the width. The contour

757 interval for the modal age is 2 month (modal age < 1 year) and 4 month (modal age >
758 1year).
759
760
761 Figure 11: Seasonal evolution of the BIRs at 80°N and 420 K as a function of source
762 time and field time.
763
764 Figure 12: Comparison of the January (black) and July (red) BIRs at some chosen
765 locations in the Northern Hemisphere. The thick lines are the mean of five BIRs, which
766 are released in January or July in 2000-2004. The thin lines are the standard deviations
767 of the five BIRs.
768
769

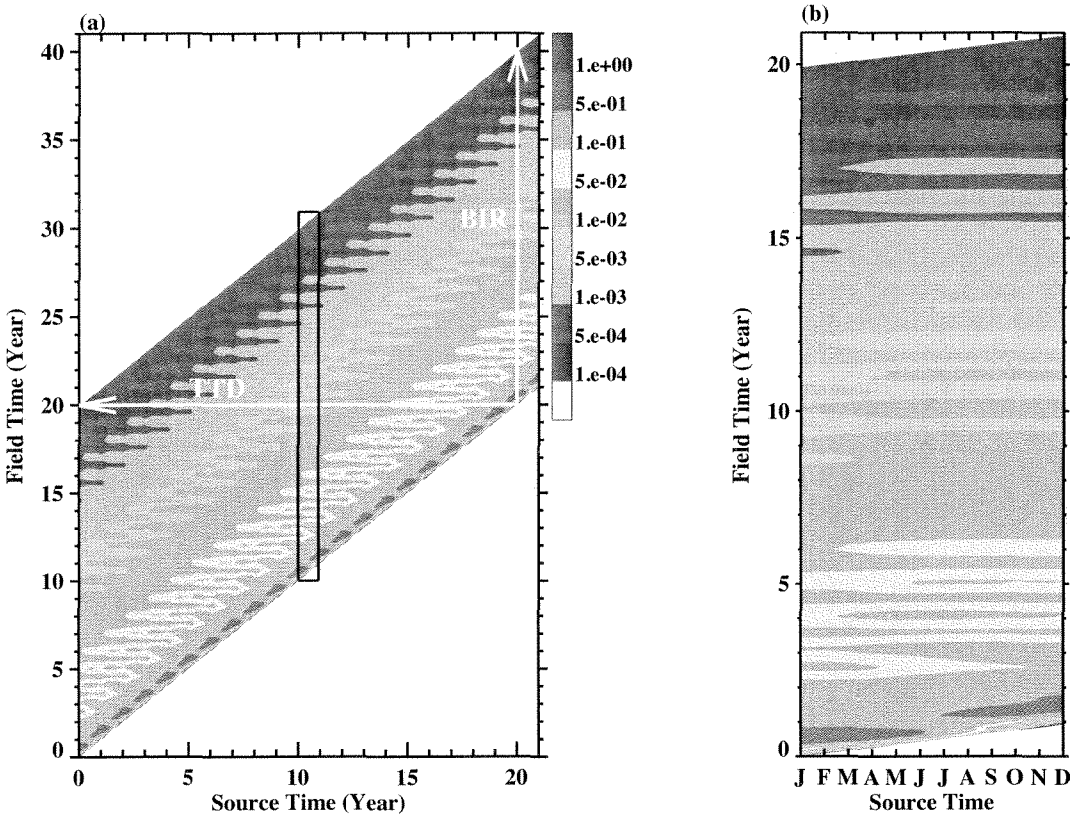

769

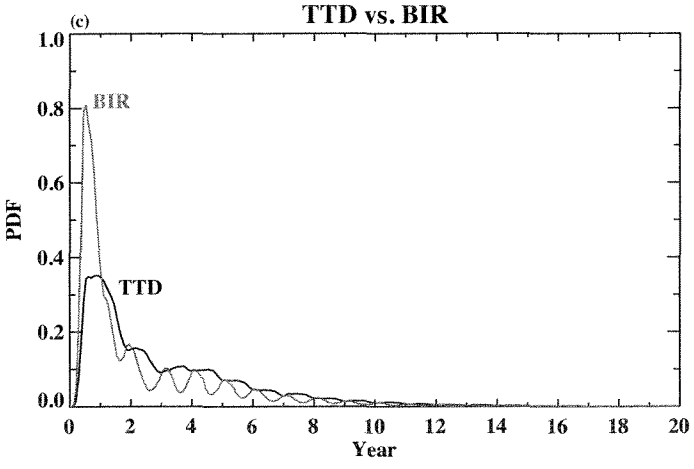

770

771

772 Figure1: Illustration of the relationship between the Transit-Time Distribution (TTD)

773 and Boundary Impulse Response (BIR). Panel (a) is a boundary propagator map at 60°N

774 and 420 K. This map is constructed from 252 vertical slices. Each vertical slice is a BIR,

775 which is fixed in source time and increases with field time. The TTD is fixed in field
776 time and increases towards older source time, i.e., a horizontal cut from right to left
777 through the boundary propagator map. An example of the BIR and TTD is shown in
778 panel (c). When constructing the boundary propagator map (a), we do not calculate all
779 the 252 BIRs. Instead we only calculate 12 BIRs with source time in each month of a
780 given year. These 12 BIR realizations (shown in panel b and in the black rectangle in
781 panel a) are then repeated every year for 20 years to form the boundary propagator map.
782

782

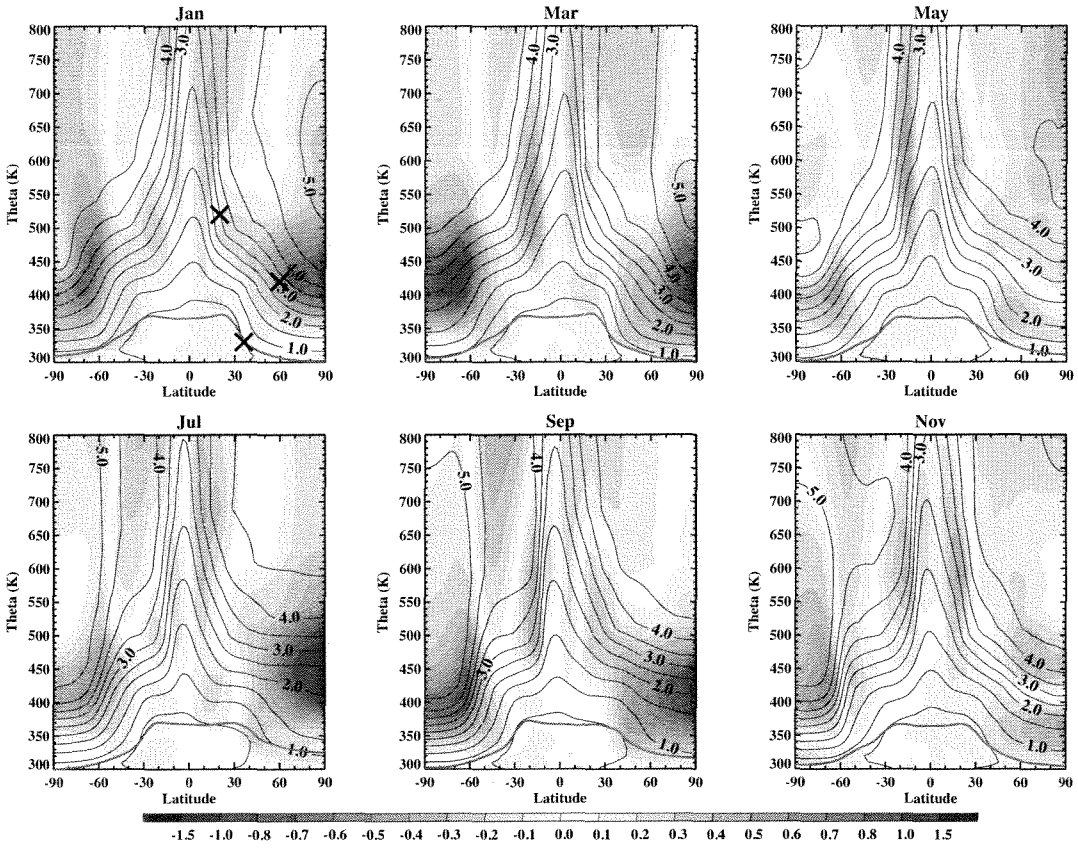

783

784

785 Figure 2: Distribution of the TTD mean age (contour) and its difference from the
786 annually averaged mean age (color) at two month intervals. The contour interval is 0.5
787 yr. The red line is the tropopause. The symbol X in the January panel indicates the
788 location of the transport barriers.

789

790

790

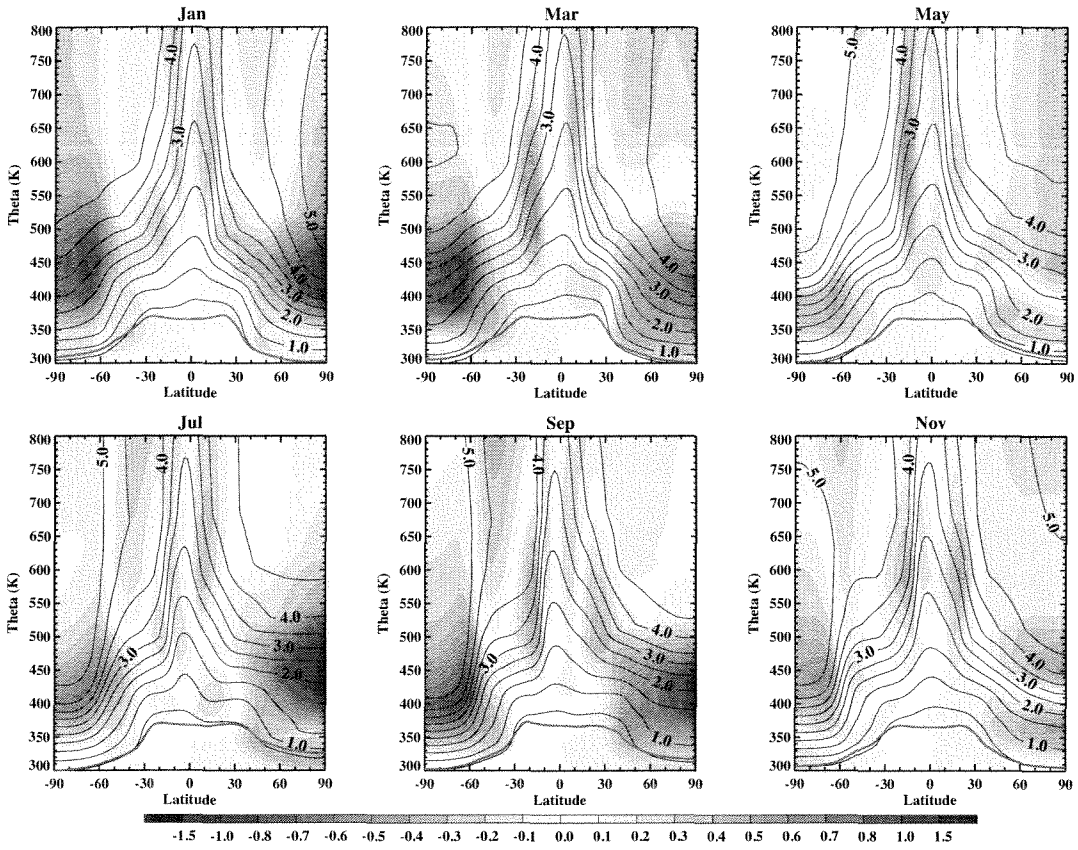

791

792

793 Figure 3: Same as Figure 2, but for the climatological mean (2000-2019) clock tracer

794 mean age.

795

795

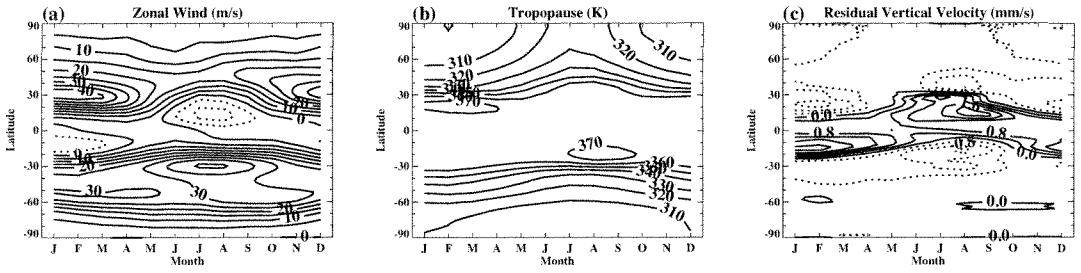

796

797

798 Figure 4: Seasonal cycle of (a) the zonal wind at 360 K; (b) the tropopause height; (c) the

799 residual vertical velocity at 360 K.

800

801

801

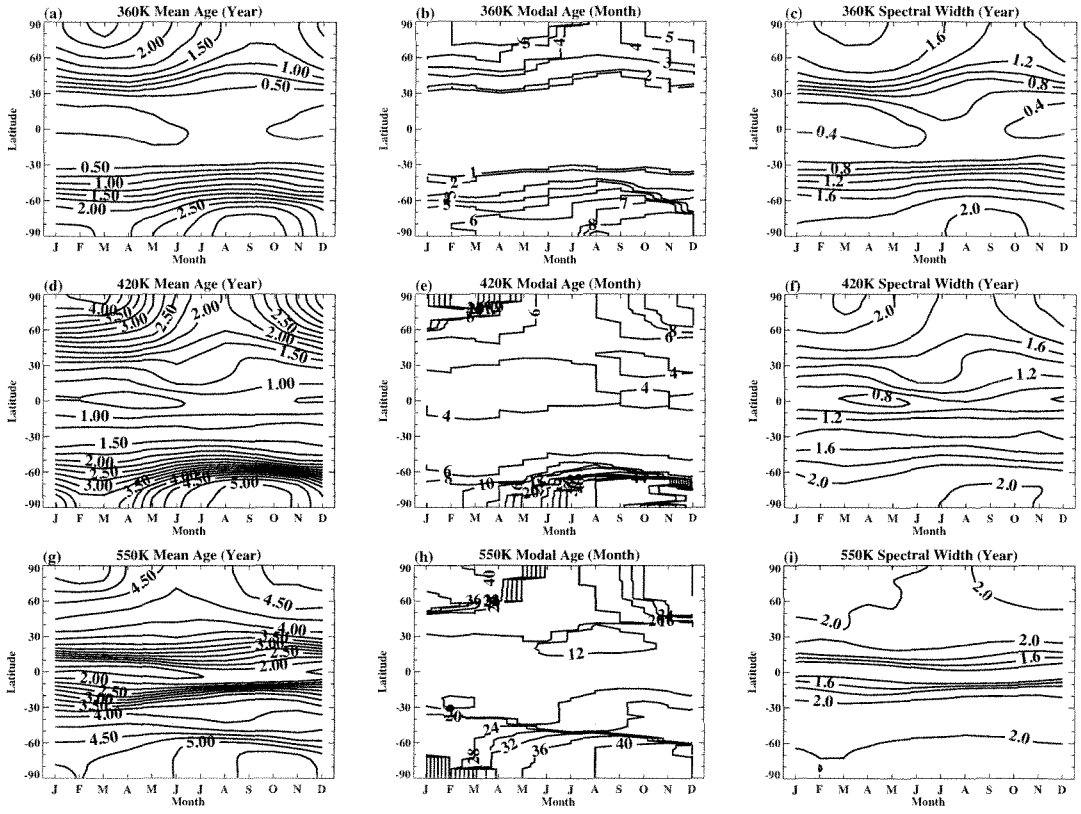

802

803

804 Figure 5: Seasonal evolution of the TTD mean age, modal age, and width at 360, 420 and
805 550 K. The contour interval is 0.25 year for the mean age and 0.2 yr for the width. The
806 unit of the modal age is month and variable contour intervals are used in different levels:
807 1 month at 360 K, 2 months (modal age < 1 yr) and 4 months (modal age > 1 yr) at 420
808 K, and 4 months at 550 K.

809

809

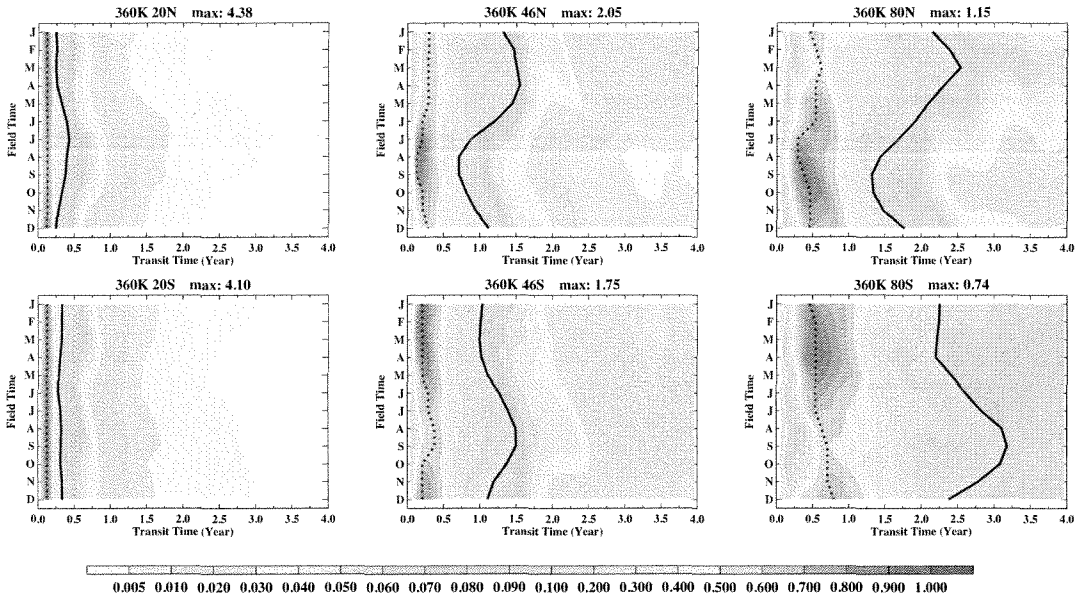

810

811

812 Figure 6: Seasonal cycle of the TTD age spectra at 20°, 46°, and 80° latitude north and
813 south at 360 K. The dotted line is the modal age and the solid line is the mean age. The
814 colors in each panel are normalized by the maximum PDF shown in the caption.

815

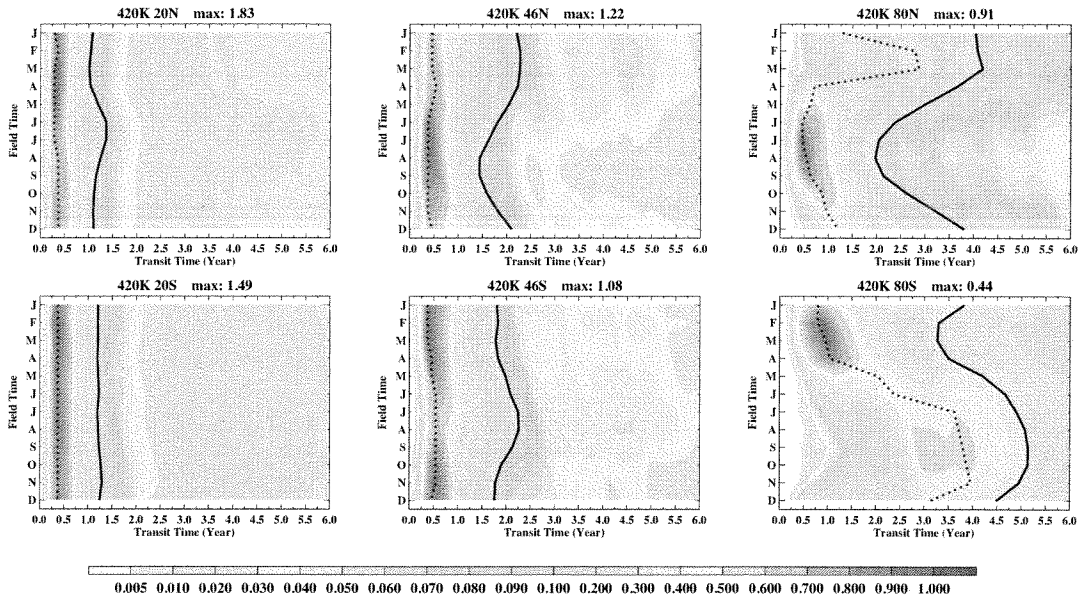

816

817

818 Figure 7: Same as Figure 6, but for 420 K.

819

819

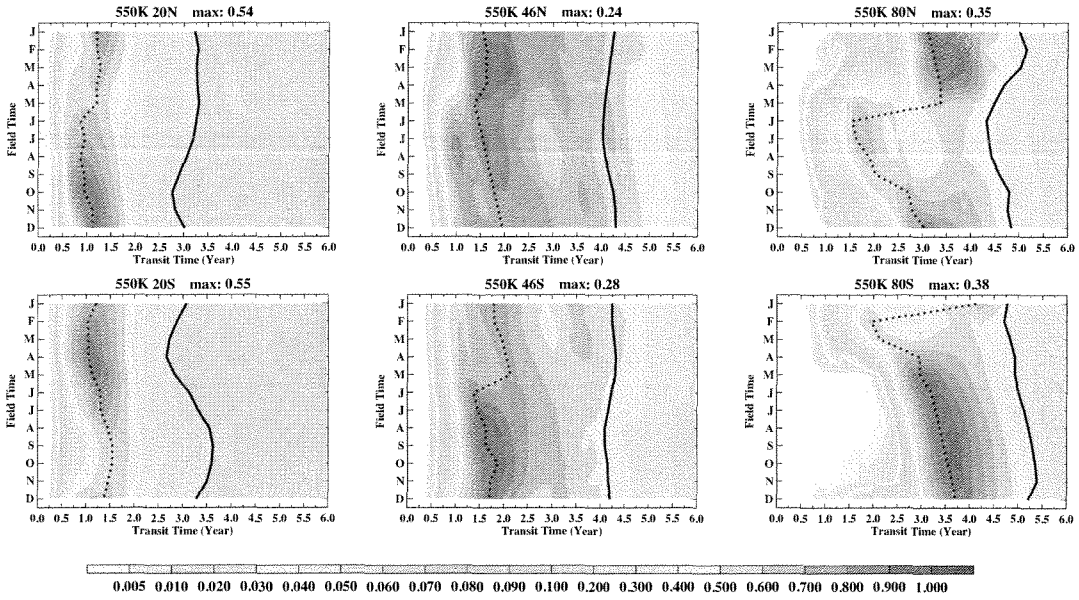

820

821

822 Figure 8: Same as Figure 6, but for 550 K.

823

823

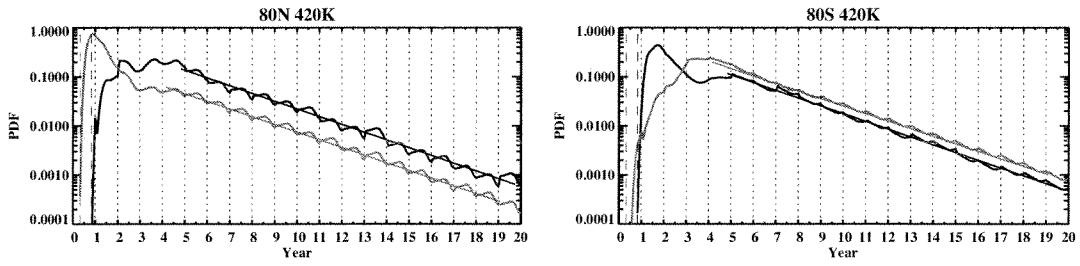

824

825

826 Figure 9: The March (black) and September (red) TTD age spectra at 80°N and S at 420
827 K. The starts of the age spectra are shifted (indicated by the thin dash lines) so that the x-
828 axis represents the season of the source time. The vertical dotted lines correspond to
829 January in source time.

830

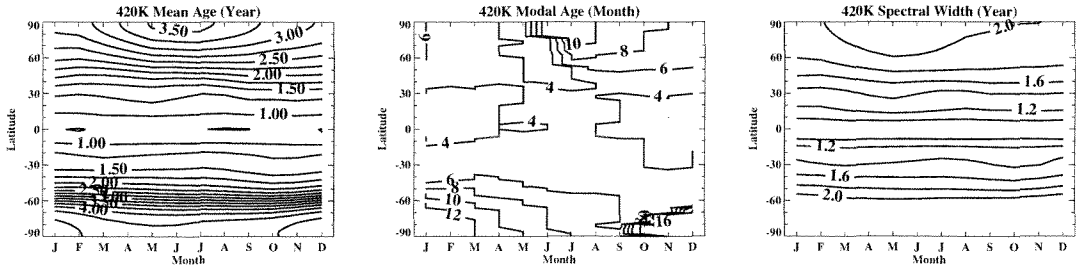

Figure 10: Seasonal evolution of the BIR mean age, modal age and width at 420 K. The contour interval is 0.25 year for the mean age and 0.2 year for the width. The contour interval for the modal age is 2 month (modal age < 1 year) and 4 month (modal age > 1year).

838

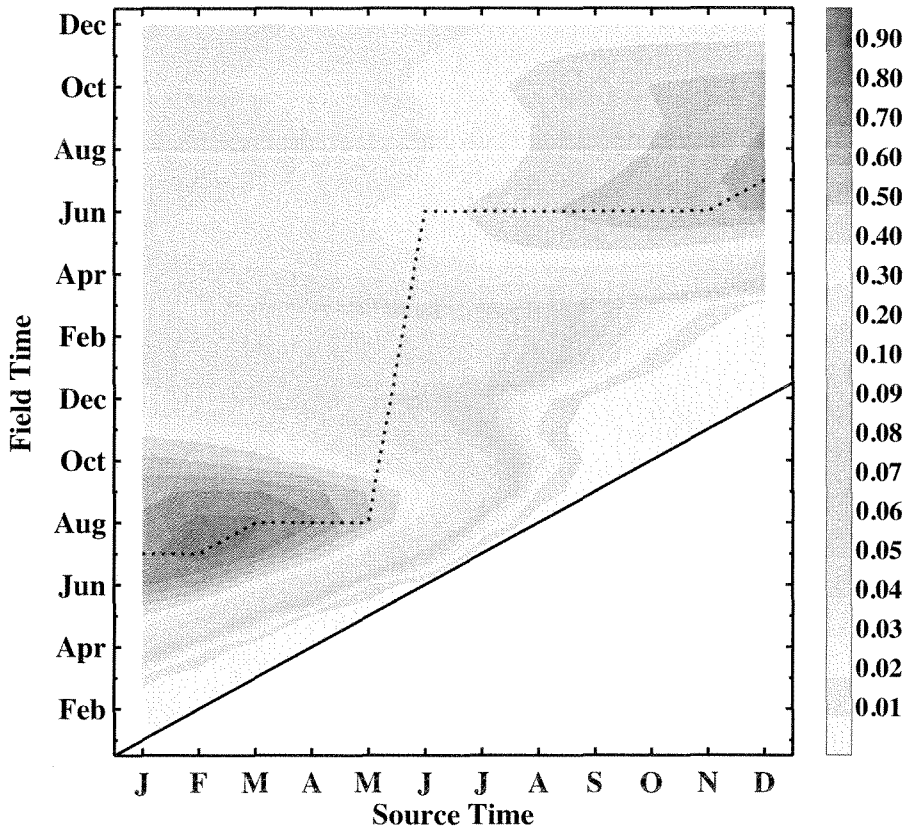

839

840

841 Figure 11: Seasonal evolution of the BIR at 80°N and 420 K as a function of source time

842 and field time.

843

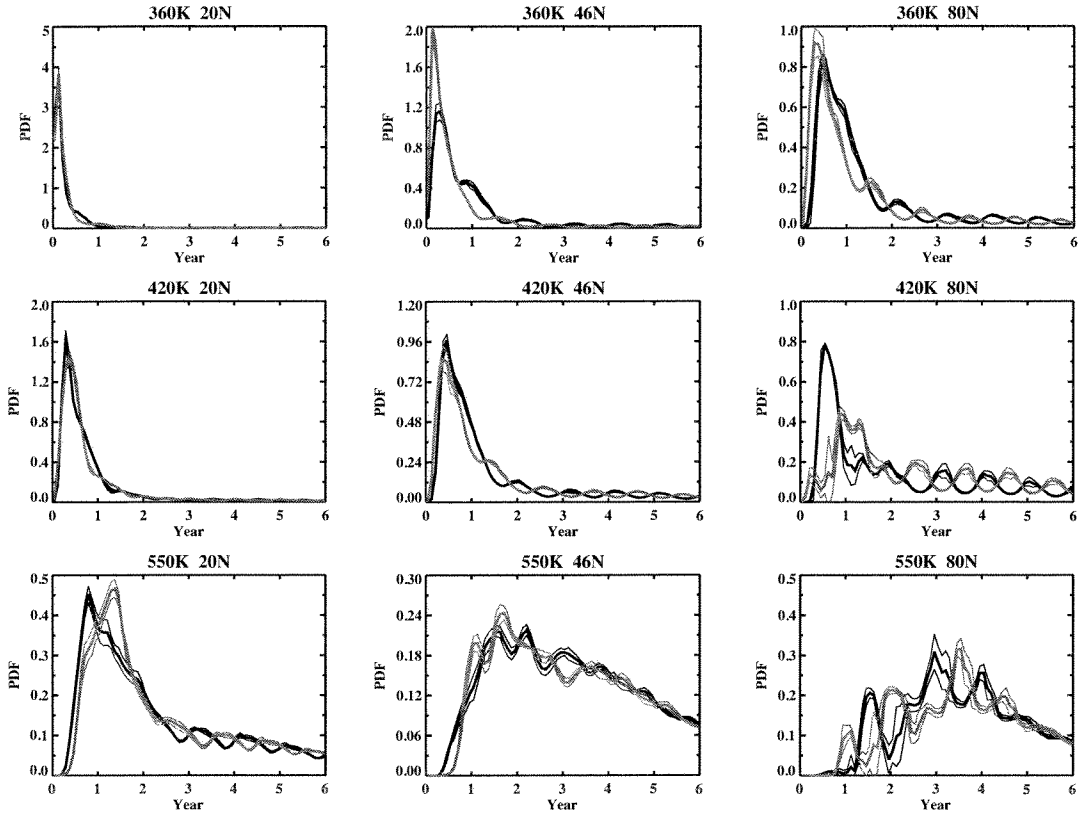

Figure 12: Comparison of the January (black) and July (red) BIRs at some chosen locations in the Northern Hemisphere. The thick lines are the mean of five BIRs, which are released in January or July in 2000-2004. The thin lines are the standard deviations of the five BIRs.